Journal of Ceramic Processing Research. Vol. 21, No. 3, pp. 319~325 (2020)
(Received 7 November 2019, Received in revised form 6 March 2020, Accepted 9 March 2020)
https://doi.org/10.36410/jcpr.2020.21.3.319

J O U R N A L O F
Ceramic Processing Research

Enhanced TE performance of $FeVSb_{1-x}Sn_x$ half-heusler matrices using zirconia vial

Rahidul Hasan[a,b], Kyu Hyoung Lee[b] and Soon-Chul Ur[a,*]
[a]*Department of Materials Science and Engineering / ReSEM, Korea National University of Transportation (KNUT), Chungju, Chungbuk 27469, Republic of Korea*
[b]*Electronic Device and Materials Laboratory (EDML), Yonsei University, Seoul 03727, Republic of Korea*

Thermoelectric and transport properties of $FeVSb_{1-x}Sn_x$ ($0.015<x<0.055$) alloys were studied with respect to types of vials (zirconia and stainless steel), Sn contents and temperature. The results were compared with the previously studied samples synthesized by using stainless-vial. All the designated compositions in current work were prepared via a mechanical alloying process using a zirconia vial. Vacuum hot pressing was conducted to consolidate the mechanically alloyed powders. F43m symmetry was being confirmed from the Rietveld refinement pattern. The phase transitions during the milling process and vacuum hot processing were investigated and the results exhibited near single half-Heusler phases with a minor portion of the second phase within the matrix. The Second phase might play a role to reduce thermal conductivity. Electrical conductivity exhibited semi-metallic behavior in all the temperature range. Carrier concentrations are found to be decreased with the increasing Sn contents and the $FeVSb_{0.955}Sn_{0.045}$ specimen showed the ZT_{max} of 0.23 at 757 K.

Keywords: Thermoelectric, X-ray Diffraction, Lattice Thermal Conductivity, Scanning Electron Microscope, Mechanical Alloying.

Introduction

Mechanical alloying (MA) process is a well-known high energy milling technique that can produce ultrafine microstructures which can be controlled during the progress of the milling [1]. It has superior advantages over other traditional processes; for instance, it may help to produce alloys that are difficult to produce applying conventional metallurgical techniques, namely casting and forging [2, 3]. Regarding this, MA can be utilized for elements with a low melting point which may suffer from sublimation during processing. Despite these benefits, there are few drawbacks of the MA process which may generate problems during the synthesizing process. One important effect that we suffered previously was the contamination of the foreign elements from stainless-steel vial during the milling [4]. It made the desired half-Heusler (HH) system unstable, causing a negative doping effect. To overcome such problems, zirconia vial was used in order to prevent the incorporation of foreign elements from the vial.

Thermoelectric (TE) generators open a feasible way to reduce the dependency of fossil fuels and greenhouse gas emissions by converting waste heat into electricity [5, 6]. However, the large-scale applications were not possible yet because of moderate conversion efficiencies and high cost of the materials [7, 8]. Generally, the TE material performance is derived from, $ZT = (\alpha^2\sigma T)/(\kappa_{lat.}+\kappa_{el.}) = (PF/\kappa)T$. It is obvious that an efficient TE material should have high α (Seebeck coefficient), σ (electrical conductivity) but low κ (thermal conductivity), $\kappa_{lat.}$ (lattice thermal conductivity) and $\kappa_{el.}$ (thermal conductivity due to electronic contribution) at the applicable temperature, T. However, it is highly challenging to get high ZT because of the inter-relation of these ZT parameters [9].

Half-Heusler (HH) alloys are the new addition in renewable energy materials and could become an appropriate candidate for TE devices. HH materials have advantages over other TE materials because of its high-temperature strength, cheap ingredients and ease of synthesis process. HH alloys showed improved TE efficiency from intermediate to high-temperature waste heat conversion [10]. Generally, HH has considerable PF at 300 K. It is the major merit point of getting high efficiency. Till today, the best TE efficiency was observed from the HH alloys of ZrNiSn, ZrCoSb, and NbFeSb in the range of ZT = 1~1.5 [11-15]. Ferluccio et al. showed that NbCoSb HH also produced $ZT \approx 1$ when it occupied vacancies at the Nb site [16]. Zhu et al. revealed that TE efficiency in HH alloys was limited due to large lattice thermal conductivity ($\kappa_{lat.}$) around 10~13 $Wm^{-1}K^{-1}$ at 300 K [17]. Recently, FeVSb HH alloy has gained research interest owing to its high PF value though it had a relatively high κ value around 8~10 $Wm^{-1}K^{-1}$ [18]. Hence, the reduction of κ is one of the main objectives to get high ZT in FeVSb alloys.

*Corresponding author:
Tel : +82-43-841-5385
E-mail: scur@ut.ac.kr

For achieving optimum efficiency, doping in the FeVSb HH system may reduce the thermal conductivity barrier [19]. Mass scattering process may be one of the efficient ways to reduce thermal conductivities in the HH system which may reduce the $\kappa_{lat.}$ around 4~5 $Wm^{-1}K^{-1}$ [20]. Recently, Zou *et al.* stated that κ could be reduced by boundary scattering engineering [21]. Stadnyk et al. studied the $Fe_{1-x}Cu_xVSb$ matrix and found metallic conductivity at elevated temperature owing to a sequential-shift in Fermi level to the conduction band [22]. Some of the previously reported highly efficient thermoelectric materials are *p*-type $ZrCoBi_{0.65}Sb_{0.15}Sn_{0.20}$ half-Heusler ($ZT \approx 1.42$ at 973 K) [23], *p*-type endoaxially nanostructured PbTe ($ZT \approx 2.2$ at 915K) [24], Bismuth-doped GeTe ($ZT \approx 1.8$ at 722 K) [25], Skutterudite $DDyFe_3CoSb_{12}$ ($ZT > 1.3$ at 773 K) [26] and Bismuth Chalcogenides, Bi_2Te_3/Sb_2Te_3 super-lattice ($ZT \approx 2.4$ at 300 K) [27].

For the investigation of the TE properties of $FeVSb_{1-x}Sn_x$ ($0.015<x<0.055$) alloys, a controlled MA process was utilized with subsequent vacuum hot pressing (VHP). Sn was used as an effective dopant for this novel system and the result was compared with the previous study for which stainless steel vial was used during milling.

Experimental Procedure

$FeVSb_{1-x}Sn_x$ HH systems were synthesized by MA process using the stoichiometric powder mixtures of Fe (63 μm), V (75 μm), Sb (45 μm) and Sn (63 μm) and all the powders were 99.9% pure. MA process was carried out using a zirconia vial in a vibratory mechanical mill for 6 h. The Speed of the mill was kept constant at 1,080 rpm throughout the process. 5 mm diameter zirconia ceramic balls were used to avoid contamination. A 325-mesh dry sieve was used for the sieving of MAed powders. Consolidation of the MAed powders was carried out using VHP at 70 MPa pressure and at 1173K temperature for 2 h. Every process was carried out under Ar-atmosphere to avoid contamination.

A particle size analyzer (PSA) was applied to get the particle size and the data were confirmed by SEM. Phase transformation of MAed powders and VHPed samples were studied by XRD. A scanning electron microscope (SEM) was employed to analyze the micro-structures of the specimens. α and σ were measured by the 4-probe method using ZEM-3. $3\times3\times10$ mm^3 rectangular samples were prepared for conducting properties measurement and $10\Phi\times1$ mm spherical disk was for thermal diffusivity measurements. Heat transfer was captured by a laser flash instrument using a TC-9000H. The density of the specimens was calculated on the basis of the Archimedes principle. Hall measurements were taken by the instrument Modified Keithley 7065 (USA) using the Van der Pauw method. Rietveld refine-ment plot was produced using the py-GSAS-II program.

Results and Discussion

Generally, the particle size of a sample decreases when doped with elements of a smaller ionic radius, which replaces the larger ions from the specimen [28]. As-MAed powders are shown to be near-spherical shape as in typical MA process and approximated particle sizes are found to be less than 10 μm (Fig. 1). There is no considerable change of particle morphology that

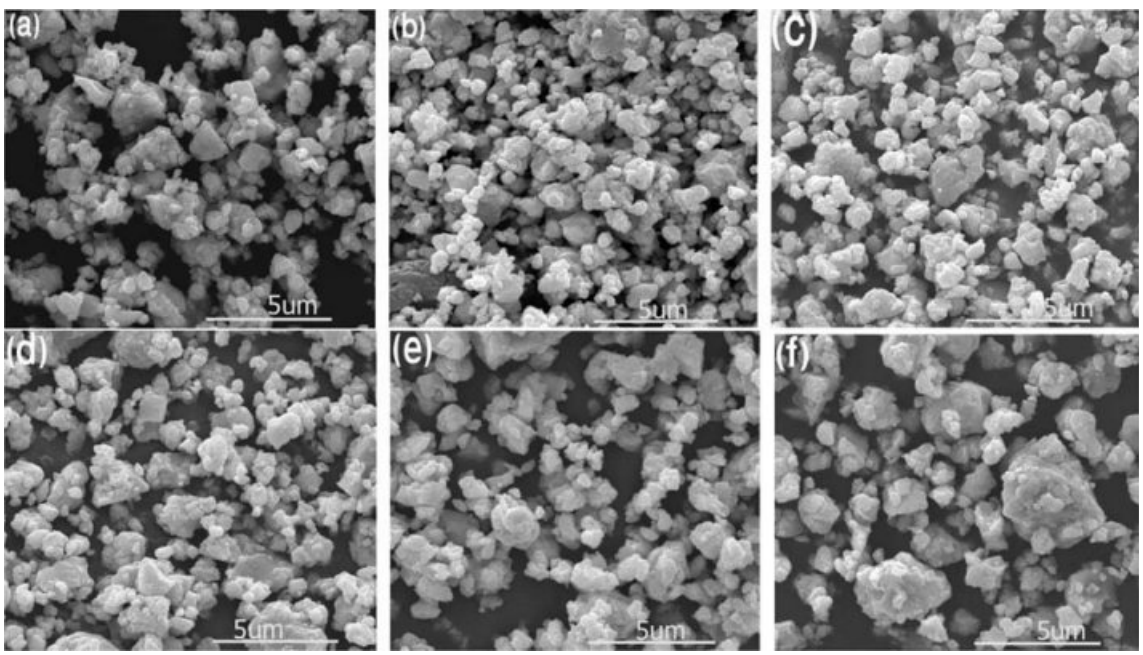

Fig. 1. Microstructures of powder specimens mill for 6 h; (a) 0 mol%, (b) 1.5 mol%, (c) 2.5 mol%, (d) 3.5 mol%, (e) 4.5 mol%, and (f) 5.5 mol%.

might be due to the use of fractional doping concentration.

XRD patterns during milling are shown in Fig. 2(a) with respect to time, and Fig. 2(b) shows the XRD curves of VHPed samples synthesized by the MA process using zirconia vial. HH phases were coming out after 4 h of milling and the remnant part of the HH phase developed during VHP [29]. Two-second phases of FeSn and Fe_2VSn were found in as-milled powders. Among these second phases, FeSn disappeared; however, Fe_2VSn still remained after VHP. Near single HH phases are dominating in VHPed samples though a fraction of the second phase (Fe_2VSn) remains, which is in agreement with our previous study [4], (Fig. 2(b)). The Rietveld refinement of the bulk samples (Fig. 2(c)) also confirms the presence of single-phase with F**4**3m symmetry.

Lattice parameters of the various compositions are depicted in Fig. 3(a). It is quite evident that the lattice

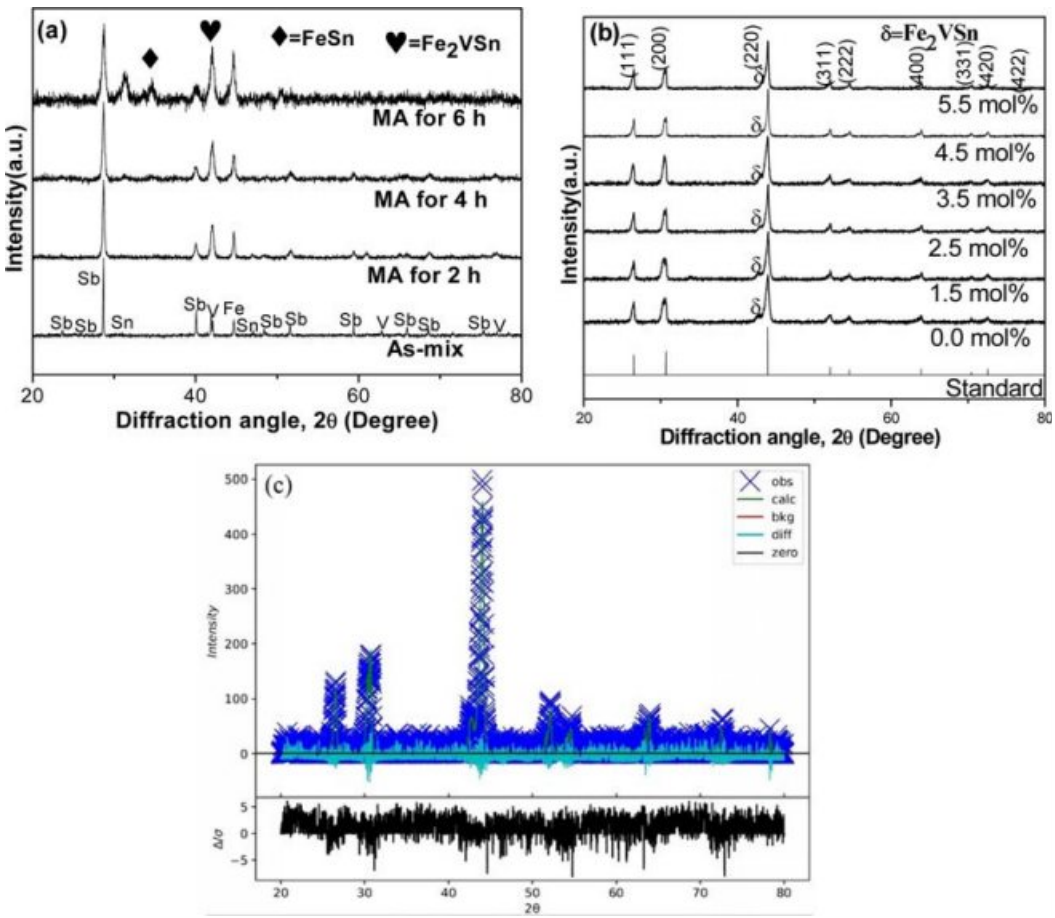

Fig. 2. (a) XRD patterns for $FeVSb_{0.945}Sn_{0.055}$ during milling which represents other samples, (b) $FeVSb_{1-x}Sn_x$ (x=0.0~0.055) HH phases applying MA process using zirconia vial, and (c) representative Rietveld refinement of bulk sample x=4.5 mol%.

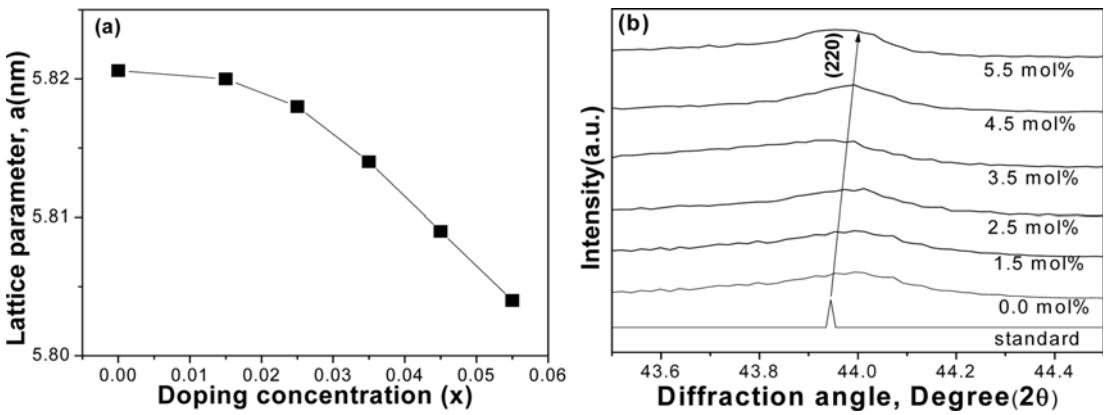

Fig. 3. Crystal structure variations of VHPed samples; (a) lattice parameter, and (b) peak shifting to the greater diffraction angle.

parameters were slightly decreased with the increase of Sn concentrations. Generally, decreasing of lattice parameters could shift the diffraction peak (220) to the greater angle [21]. The substitution of smaller Sn^{+4} (0.69 Å) from the larger Sb^{+3} (0.76 Å) might be responsible for this effect, as shown in Fig. 3(b). The second phase might have played a role to decrease the lattice constant with the increase of Sn concentration [30]. The relative density is found to be quite lower than our expectation (~95%, Fig. 5.). It might be due to the formation of a small fraction of voids during hot-consolidation.

SEM images for VHPed samples are represented by Fig. 4. Generally, the MA process gave rise to ultrafine microstructure [1]. In this study, the average grain size could not be detected accurately from the microstructures. However, the microstructures showed that the approximate grain/particle size could be less than 10 μm, which is a usual feature of MA and VHP [31]. From the SEM images, it can be presumed to be prior particle boundaries or grain boundaries present in the samples but we are not sure which one it is in this set of experiments. Since the doping concentration used was very low, it didn't show any significant change in grain morphology as well.

Fig. 6 illustrates the Seebeck coefficient of the VHPed samples produced by the MA process using zirconia vial. The values of α were detected negative in sign, which in turn reveal that the present charge carriers were electrons. Notice that, the absolute value of α increases with increasing doping concentration at

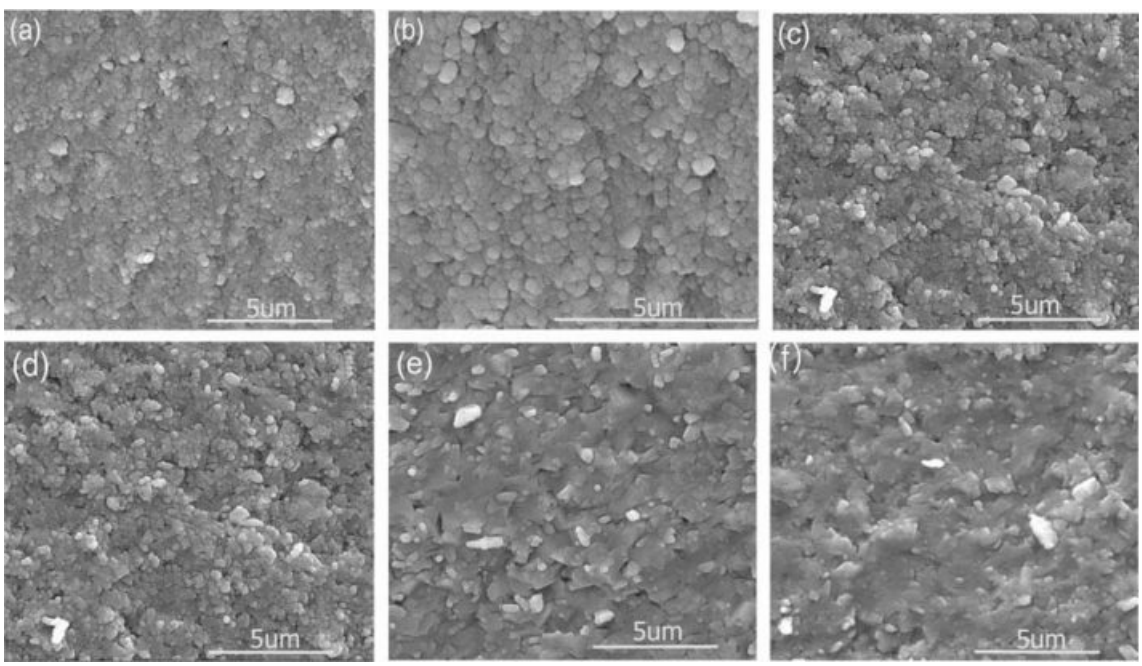

Fig. 4. Scanning electron microscope images of the various Sn-doped VHPed samples: (a) 0 mol%, (b) 1.5 mol%, (c) 2.5 mol%, (d) 3.5 mol%, (e) 4.5 mol%, and (f) 5.5 mol%.

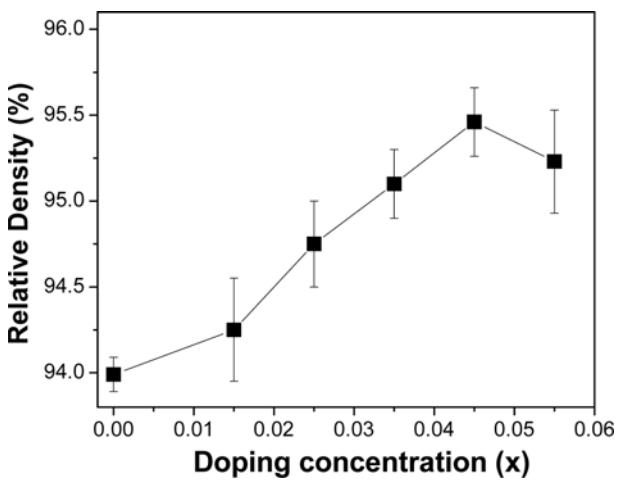

Fig. 5. The relative density of the bulk $FeVSb_{1-x}Sn_x$ HH systems against the doping concentration

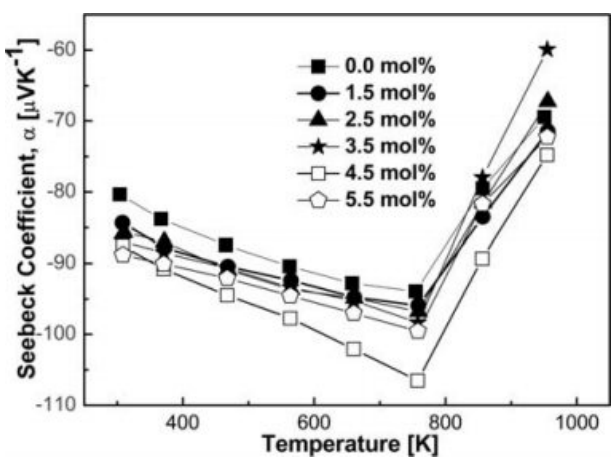

Fig. 6. The Seebeck coefficient of $FeVSb_{1-x}Sn_x$ HH systems as a function of T, processed by MA process using zirconia vial

300 K in the MA process using zirconia vial. The Hall measurement data from Table 1 also supports this increase in the absolute value of α. Generally, α increases with the decrease of carrier concentration. On the contrary, the absolute value of α decreased with increasing Sn contents during milling, possibly due to the undesired incorporation of vial composition in the MA process using stainless-steel vial [4], which was confirmed by EDS analysis. Shashanka and Chaira *et al.* also reported such incorporation in their work [32]. There was no evidence of incorporation of the foreign elements from vial found in controlled MA process using zirconia vial in this study, which is shown in Table 2. Moreover, the absolute value of α was increased with increasing T and with doping concentration in the controlled MA process using zirconia vial possibly owing to the intrinsic excitation of the bands [33, 34]. The highest absolute value of α was found to be 106 μVK^{-1} at 758 K, which was observed for 4.5 mol% in the MA process using zirconia vial indicated well-controlled composition of HH phase.

Fig. 7 showed the measured σ for controlled MA process. The values of σ showed a similar trend to our previous work [4] after adding dopants. σ was found to be decreased in the MA process using both zirconia and stainless-steel vial with increasing Sn contents. In both cases, σ increased with increasing T, which indicated the inherent semi-metallic behavior. This increasing trend of σ might have forced the Fermi band to the higher conduction band by the thermal excitement of charge carriers within the bandgap [35].

Fig. 8(a) and 8(b) represent $\kappa_{lat.}$ and κ with respect to time and doping elements. Thermal energy is transferred by the thermalized electrons in the conduction band and lattice vibration (phonon). The total thermal conductivity of a material system can be expressed by the following equation, $\kappa = \kappa_{lat.} + \kappa_{el}$. Both κ and $\kappa_{lat.}$ of $FeVSb_{1-x}Sn_x$ were found to be decreased significantly with increasing Sn contents. Possibly, enhanced phonon scattering could play a major role in this decrease of κ and $\kappa_{lat.}$ [36]. Additionally, highly dense grain boundaries might form because of the expected small grain size (~10 μm) [37]. Consequently, the scattering of phonon could take place at grain boundaries which might produce a favorable path to the reduction of $\kappa_{lat.}$. A similar tendency was experienced for κ of all $FeVSb_{1-x}Sn_x$ HH samples. There is a slight difference found between κ and $\kappa_{lat.}$ due to the very low value of $\kappa_{el.}$ of $FeVSb_{1-x}Sn_x$ HH alloys. Though $\kappa_{lat.}$ is found considerably low; however, it cannot be ignored for good TE devices. A portion of the second phase could also be responsible for this decreasing value of κ [38]. The origin of the cause in the differences of thermal conductivity and lattice thermal conductivity might

Table 1. Measured Hall data of the bulk $FeVSb_{1-x}Sn_x$ HH systems at room temperature synthesized by using zirconia vial.

Nominal composition	Hall coefficient (cm^3/C)	Hall Mobility (cm^2/Vsec)	Carrier conc. (cm^{-3})
x=0.000	-0.191	285.52	7.51×10^{20}
x=0.015	-0.212	312.52	6.32×10^{20}
x=0.025	-0.535	402.37	5.97×10^{20}
x=0.035	-0.719	456.91	5.79×10^{20}
x=0.045	-0.854	512.80	5.23×10^{20}
x=0.055	-1.054	522.13	4.68×10^{20}

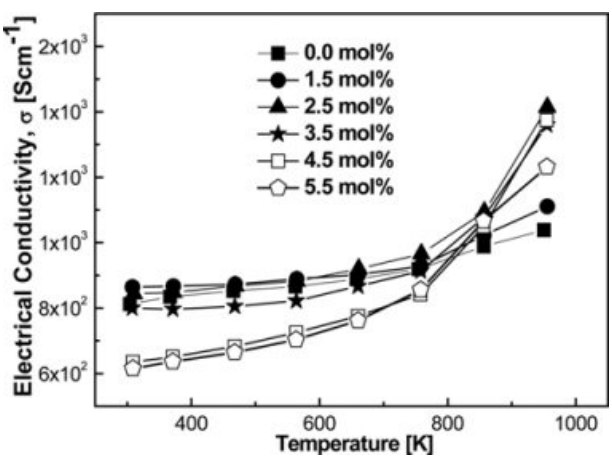

Fig. 7. Temperature dependence of σ values as a function of T for the MA process using zirconia vial

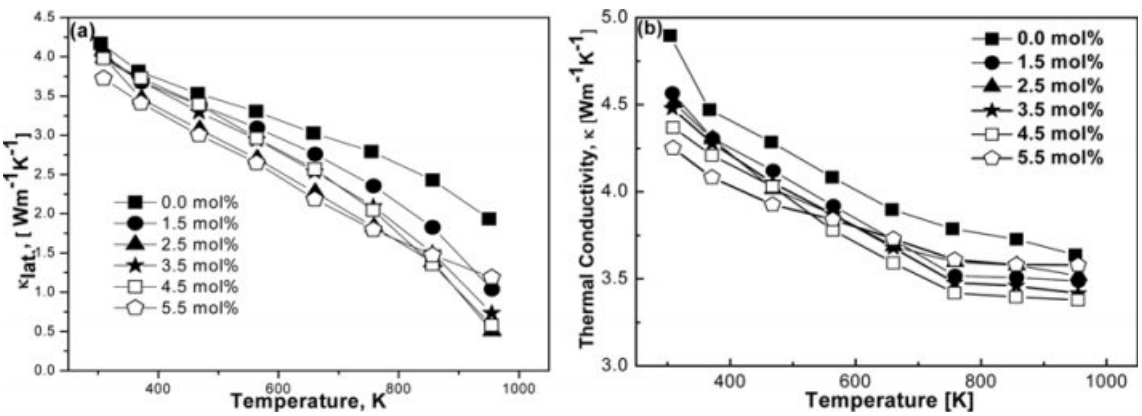

Fig. 8. Calculated (a) $\kappa_{lat.}$, (b) κ of the VHPed samples produced by MA process using zirconia vial.

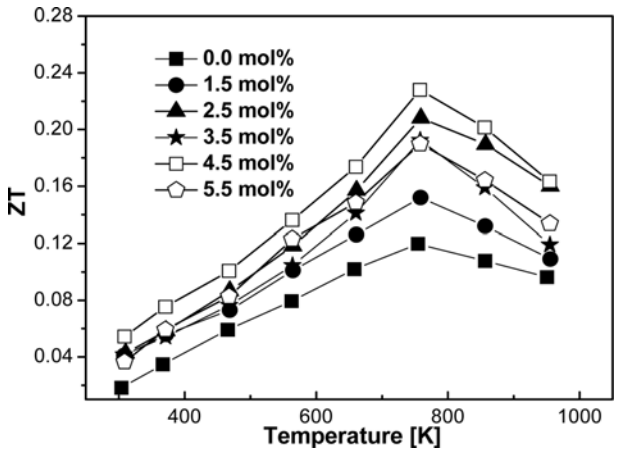

Fig. 9. Calculated ZT of VHPed $FeVSb_{1-x}Sn_x$ specimens for the MA process using zirconia vial.

Table 2. EDS analysis of the VHPed samples synthesized by the MA process using zirconia and stainless-steel vial.

Elements	MA process using zirconia vial (at.%), doping concentration, x=4.5 mol%	MA process using stainless steel vial (at.%), doping concentration, x=1 mol%
Sb	20.63	20.54
Fe	36.44	36.33
Sn	10.31	10.15
V	32.62	32.50
Ni	0.00	0.06
Cr	0.00	0.42
Total	100.00	100.00

be the reduction of the acoustic phonon bandwidth, consequently lowering the acoustic phonon group velocities [39], which might decrease the lattice thermal conductivity.

Fig. 9. indicates the ZT value calculated from α, σ, and κ for the MA process using zirconia vial. Comparing the MA process between zirconia vial and stainless-steel vial, the former produced a much higher ZT compared to ref. [4], which is clearly seen from the figure. Generally, a sample with high relative density possesses the maximum ZT and that is evident for $FeVSb_{0.955}Sn_{0.045}$ at 757 K. The corresponding $ZT_{max}\approx0.23$ was calculated because of relatively high α and low κ, which suggest that ZT can be further improved by careful tuning of appropriate dopant. If κ might have reduced further by applying multiple substitutions and/or small grain formation, ZT could be enhanced to unity which is in good accordance with Codrin *et al.* [25].

Conclusions

$FeVSb_{1-x}Sn_x$ (x=0.015~0.055) HH compositions were fabricated by the MA process using zirconia vial. A subsequent VHP was required to consolidate the powders. After MA and VHP, all the compositions produced near single HH phases. In this study, TE properties of the MAed materials processed using zirconia vial and stainless-steel vial were evaluated as a function of doping concentration and T and compared between them. It was found that the incorporation of foreign elements from stainless-steel vial reduced the absolute value of α and increased the κ by negative doping effect. On the other hand, α was not being affected by impurities in the MA process using zirconia vial, leading to a relatively higher absolute value of α of 106 μVK^{-1} at 758 K for the optimum composition. κ reduced comprehensively for the MA process using zirconia vial, possibly due to enhanced phonon scattering due to doped with Sn and second phase interaction. It was observed that Sn-doping in FeVSb HH phases synthesized by the MA process using zirconia vial reduced κ to its lowest value of 3.38 $Wm^{-1}K^{-1}$ from intrinsic FeVSb (~8 $Wm^{-1}K^{-1}$). A ZT_{max} of 0.23 was being calculated for $FeVSb_{0.955}Sn_{0.045}$ at 757 K using zirconia vial, which is a much-improved value compared to the MA process using stainless-steel vial [4]. The lower $\kappa_{lat.}$ and relatively high magnitude of α played the main part to reach this ZT_{max}. Further improvements in TE efficiency it might be possible by the multi-doping technique.

Acknowledgments

This research was supported by the Korea Basic Science Institute grant funded by the Ministry of Education (grant no. 2019R1A6C1010047).

References

1. S.-C. Ur, H. Choo, D.B. Lee, and P. Nash, Metals and Materials. 6[5] (2000) 435-440.
2. M. Blair and T.L. Stevens, in "Steel Castings Handbook" (ASM International, Ohio, USA, 1995) p.71.
3. E.P. DeGarmo, J.T. Black and R.A. Kohser, in "Solution Manuals to Accompany-Materials and Process in Manufacturing" (John Wiley and Sons Ltd, 2003) p.122.
4. R. Hasan and S.-C. Ur, J. of Trans. Electr. Electron. Mater. 19[2] (2018) 106-111.
5. D.M. Rowe, in "Thermoelectrics and Its Energy Harvesting" (CRC Press, 2012) p.80.
6. T.M. Tritt, Annu. Rev. Mater. Res. 41[1] (2011) 433-448.
7. M. Zebarjadi, K. Esfarjani, M.S. Dresselhaus, Z.F. Ren, and G. Chen, Energy Environ. Sci. 5[1] (2012) 5147-5162.
8. W.S. Liu, Q. Jie, H.S. Kim, Z.F. Ren, Acta Mater. 87 (2015) 357-376.
9. G.J. Snyder and E.S. Toberer, Nature Materials. 7[2] (2008) 105-114.
10. S.A. Barczak, J. Buckman, R.I. Smith, A.R. Baker, E. Don, I. Forbes, and J.W.G. Bos, Materials. 11[4] (2018) 536.
11. L. Chen, S. Gao, X. Zeng, A.M. Dehkordi, T.M. Tritt, and S.J. Poon, Appl. Phys. Lett. 107[4] (2015) 041902.
12. M. Gurth, G. Rogl, V.V. Romaka, A. Grytsiv, E. Bauer, and P. Rogl, Acta Mater. 104 (2016) 210-222.

13. X.A. Yan, G. Joshi, W.S. Liu, Y.C. Lan, H. Wang, S. Lee, J.W. Simonson, S.J. Poon, T.M. Tritt, G. Chen, and Z.F. Ren, Nano Lett. 11[2] (2011) 556-560.
14. E. Rausch, B. Balke, T. Deschauer, S. Ouardi, and C. Felser, APL Mater. 3[4] (2015) 105.
15. C.G. Fu, S.Q. Bai, Y.T. Liu, Y.S. Tang, L.D. Chen, X.B. Zhao, and T.J. Zhu, Nature Communications. 6[1] (2015) 6888.
16. D.A. Ferluccio, R.I. Smith, J. Buckman, and J.W.G. Bos, Phys. Chem. Chem. Phys. 20[6] (2018) 3979-3987.
17. T.J. Zhu, C.G. Fu, H.H. Xie, Y.T. Liu, and X.B. Zhao, Adv. Energy Mater. 5[19] (2015) 1500588.
18. A. Yamamoto and T. Takeuchi, J. of Elec. Materi. 46[5] (2017) 3200-3206.
19. H. Hohl, A.P. Ramirez, C. Goldmann, G. Ernst, B. Wolfing, and E. Bucher, J. Phys.: Condens. Matter. 11[7] (1999) 1697-1709.
20. L.D. Zhao, S.H. Lo, Y.S. Zhang, H. Sun, G.J. Tan, C. Uher, C. Wolverton, V.P. Dravid, and M.G. Kanatzidis, Nature. 508[7496] (2014) 373-377.
21. M. Zou, J.F. Li, and T. Kita, J. of Sol. Stat. Chem. 198 (2013) 125-130.
22. Y. Stadnyk, A. Horyn, V. Sechovsky, L. Romaka, Y. Mudryk, J. Tobola, T. Stopa, S. Kaprzyk, and A. Kolomiets, J. Alloys Compd. 402 (2005) 30-35.
23. H. Zhu, R. He, J. Mao, Q. Zhu, C. Li, J. Sun, W. Ren, Y. Wang, Z. Liu, Z. Tang, A. Sotnikov, Z. Wang, D. Broido, D.J. Singh, G. Chen, K. Nielsch, and Z. Ren, Nature Communications. 9[1] (2018) 2497.
24. K. Biswas, J. He, I. D. Blum, C.-I. Wu, T.P. Hogan, D.N. Seidman, V.P. Dravid, and M.G. Kanatzidid, Nature 489[7416] (2012) 414-418.
25. J. Li, Z. Chen, X. Zhang, Y. Sun, J. Yang, and Y. Pei, NPG Asia Mater. 9[3] (2017) e353.
26. G. Rogl, A. Grytsiv, R. Anbalagan, J. Bursik, M. Kerber, E. Schaflur, M. Zehetbauer, E. Bauer, and P. Rogl, Acta Mater. 159 (2018) 352-363.
27. R. Venkatasubramanian, E. Siiviola, T. Colpitts, and B. O'Quinn, Nature. 413[6856] (2001) 597-602.
28. I.-H. Kim, J.-C. Kweon, Y.-G. Lee, M.-S. Yoon, S.-L. Ryu, W.-G. Kim, and S.-C. Ur, Mater. Sci. Forum. 658 (2010) 33-36.
29. E. Yuasa, T. Morooka, M. Tsunoda, and J. Mishima, J. of the Japan Soc. of Powd. and Powd. Metall. 42[2] (1995) 171-174.
30. K.D. Codrin, T. Yamada, A. Yamamoto, R. Sobota, M. Matsunami, and T. Takeuchi, Jpn. J. Appl. Phys. 56[11] (2017) 111202.
31. P. Jozwik and Z. Bojar, Archives of Metallurgy and Materials. 52[2] (2007) 321-327.
32. R. Shashanka and D. Chaira, in "Ball Milled Nano-Structured Stainless-Steel Powders-Fabrication and Characterization" (Educreation Publishing, 2011) p.8.
33. H.J. Goldsmid, in "Electronic refrigeration" (Pion, 1986).
34. T. Xing, R. Liu, F..Hao, P. Qiu, D. Ren, X. Shi, and L. Chen, J. Mater. Chem. C, 5[47] (2017) 12619-12628.
35. D.P. Young, P. Khalifah, R.J. Cava, and A.P. Ramirez, J. of Appl. Phys. 87[1] (2000) 317-321.
36. J.J. Gong, A.J. Hong, J. Shuai, L. Li, Z.B. Yan, Z.F. Ren, and J.-M. Liu, Phys. Chem. Chem. Phys. 18[24] (2016) 16566-16574.
37. R. Hasan and S. C. Ur, Elect. Mater. Lett. 14[6] (2018) 725-732.
38. J. Cui, G. Cai, and W. Ren, RSC Adv. 8[38] (2018) 21637-21643.
39. H. Euchner, S. Pailhès, V. M. Giordano, and M. de Boissieu, Phys. Rev. B. 97[1] (2018) 014304.